GSA Data Repository 2019222

Evidence for anoxic shallow oceans at 2.45 Ga: Implications for the rise of oxygenic photosynthesis

Birger Rasmussen, Janet R. Muhling, Nicholas J. Tosca, and Harilaos Tsikos

METHODS

Lamellae for transmission electron microscopy (TEM) analyses were cut from laminated cherts enclosing iron-silicate nanoparticles in polished thin sections. Focussed ion beam (FIB) techniques were used to prepare ~100 nm thick TEM lamellae using an *FEI Helios NanoLab G3 CX DualBeam* instrument located at the Centre for Microscopy, Characterisation and Analysis (CMCA), the University of Western Australia. The areas selected for TEM analysis were first coated with a strip of Pt, 2 µm thick to protect the surface, then trenches 7 µm deep were milled on either side of the strip using a Ga ion beam with 30 kV voltage and 9.3 nA current. The lamellae were then cut from the samples and welded to Cu TEM grids. The lamellae were thinned with the Ga ion beam at 30 kV and 0.79 nA and 0.23 nA, before cleaning at 5 kV and 41 pA, and polishing at 2 kV and 23 pA.

Transmission electron microscope data were obtained at 200 kV using an *FEI Titan G2 80–200 TEM/STEM* with *ChemiSTEM* technology located at CMCA, UWA. Bright-field TEM, High-resolution TEM (HRTEM) and high-angle annular dark-field (HAADF) STEM images were collected and processed using TIA (TEM Imaging and Analysis) software from FEI and Digital Micrograph from Gatan Incorporated. Qualitative EDS spectra (see below – Fig. DR1) and hypermaps were collected and processed using Bruker Esprit software.

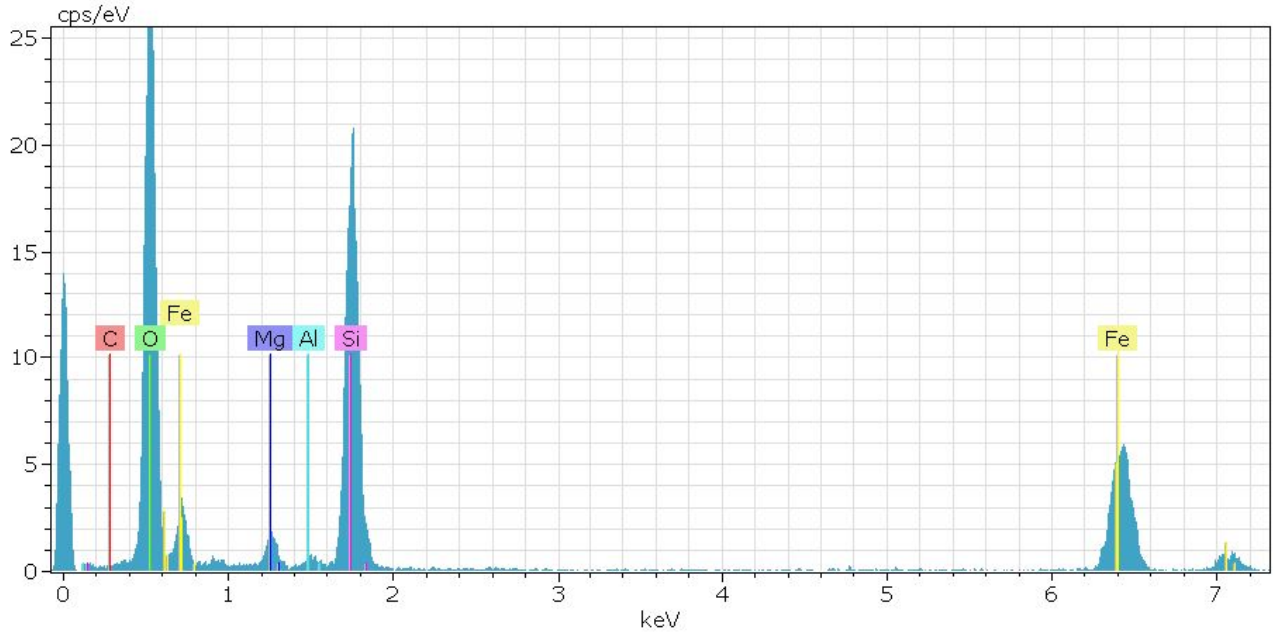

Fig. DR1. TEM EDS spectrum of iron-silicate (greenalite) nanoparticle in laminated chert.

ESTIMATES OF SEAWATER $O_2(aq)$

Greenalite precipitation rates in seawater

To estimate the conditions under which the precipitation rate of greenalite outpaced the oxidation rate of Fe(II) in a shallow Archean marine water column, we require quantitative constraints on greenalite precipitation kinetics. For this, we used data from Tosca et al. (2016) who examined greenalite nucleation from anoxic seawater solutions as a function of Fe and $SiO_2(aq)$ concentration, as well as pH. All experiments were conducted in anoxic synthetic seawater solutions which, after a given time interval, homogeneously nucleated greenalite. In all experiments from which kinetic data were derived, greenalite was the sole precipitation product (as determined by powder X-ray diffraction, FT-IR spectroscopy, thermogravimetric analysis, and TEM analysis). For all experiments, total Fe(II) and total $SiO_2(aq)$ in solution were measured over time. This allows the total Fe precipitation rate to be calculated as a function of supersaturation. Greenalite supersaturation is a convenient global parameter to represent overall precipitation rates because the overall effect of changing Fe concentration, $SiO_2(aq)$ concentration, and/or pH is encapsulated in the following equilibrium solubility relationship:

$$K_{sp(Greenalite)} = \frac{a_{Fe^{2+}}^{3} a_{SiO_2}^{2}}{a_{H^+}^{6}}$$

At non-equilibrium conditions,

$$IAP = \frac{a_{Fe^{2+}}^{3} a_{SiO_2}^{2}}{a_{H^+}^{6}}$$

The supersaturation can be expressed with the saturation index:

$$SI = \log\left(\frac{IAP}{K_{sp(Greenalite)}}\right)$$

Figure DR2 shows the total greenalite precipitation rate as a function of supersaturation (where log IAP/Ksp values are greater than 0). The total precipitation rate of greenalite from these experiments is a combination of the nucleation rate and the growth rate. However, detailed structural characterization of freshly precipitated greenalite from these experiments shows that greenalite precipitation is dominated by nucleation rather than crystal growth (Tosca et al., 2016). In other words, because of low surface energy and high solubility, the structural precursor to greenalite, which is precipitated directly from seawater, is composed of many small particles on the order of several tens to hundreds of nanometers in size, rather than few large crystals. With time and/or shallow burial, this structural precursor dehydrates and re-orders to form crystalline greenalite (Tosca et al., 2016). Because the overall precipitation rate is dominated by nucleation phenomena, we chose to fit kinetic data for greenalite precipitation with an exponential function that describes the nucleation rate (cm^{-3} sec^{-1}) of a substance from water (Lasaga, 1998).

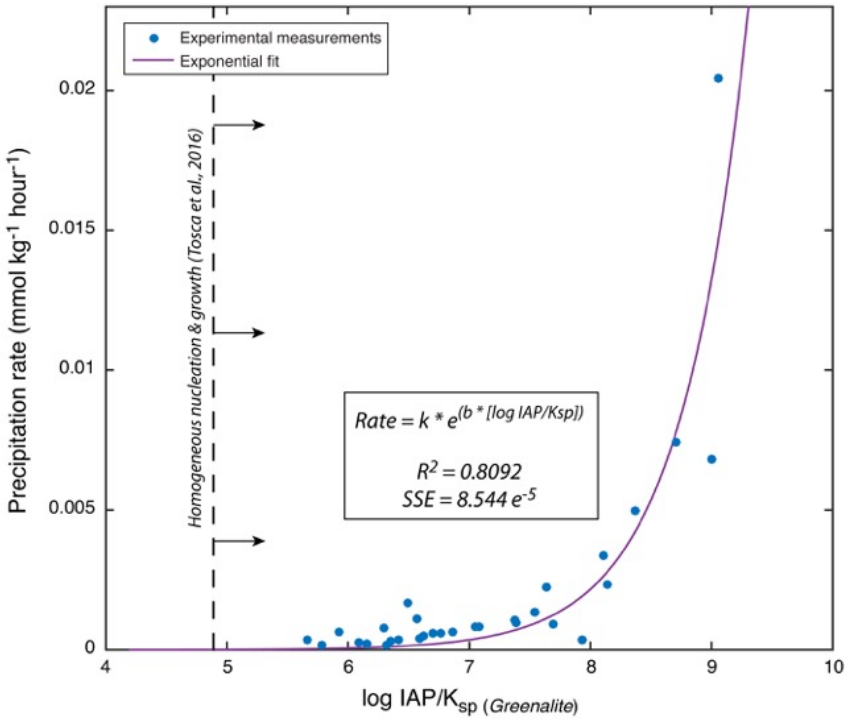

Fig. DR2. Experimentally determined greenalite precipitation rate as a function of supersaturation. Data points represent experimental measurements of greenalite precipitation rate by Tosca et al. (2016). These data define a relationship identical in form to nucleation rates predicted by kinetic theory.

Our exponential fit is a simplified form of this relationship where k is an overall rate constant and b is a factor which incorporates the surface energy and molar properties of greenalite nuclei (Fig. DR3). Although neither k or b are known a priori, or from the literature, they can be derived from our experimental data (Fig. DR2). In other words, we achieve a good fit to laboratory data by specifying an equation of a general form derived from nucleation theory. It is worth noting that precipitation rate data are limited at low values of supersaturation by the time scales at which greenalite precipitation can be observed in the laboratory. Because the nucleation rate dependence on supersaturation is a strong exponential relationship (Lasaga, 1998), we are able to identify the kinetic factors for the "critical saturation" and apparent solubility of the greenalite phase delineated by Tosca et al. (2016) - the exponential dependence of the greenalite nucleation rate means that rates are prohibitively slow at values less than this; so slow that observable increments of greenalite precipitation exceeds reasonable early diagenetic timescales.

Fe^{2+}-oxidation rates in seawater

In order realistically calculate Fe(II) oxidation rates in Archean seawater, we developed a model that incorporates the effects of pH, Fe(II) concentration, and P_{CO2}. Recent investigations of the rate of Fe(II) oxidation in natural waters (i.e., free energy concentrations and rate measurements in media of varying composition: Millero et al., 1987; Millero et al., 1989; Wehrli, 1990) have highlighted that different aqueous iron species react with dissolved oxygen at different rates. Thus, the overall Fe(II)-oxidation rate is most accurately expressed as a weighted sum of the oxidation rates of individual Fe(II) species.

Although the Fe(II)-oxidation rate in modern seawater has been measured with significant precision, one key difference likely to influence rates in Archean seawater is the role of dissolved CO_2. This is likely to influence Fe(II)-oxidation rates to a greater degree than $SiO_2(aq)$, based on the estimated stability constants of Fe(II)-carbonate and silicate complexes, respectively, and because $SiO_2(aq)$ species are uncharged in aqueous solutions at pH <9. Experimental measurements of Fe(II)-oxidation rate in carbonated seawater have made it clear that CO_2 does, in fact, enhance the Fe(II) oxidation rates (Millero et al., 1987).

To take the effect of dissolved CO_2 into account, we used a speciation model for Fe(II)-oxidation developed by King (1998). This model uses a Pitzer ion interaction framework to calculate the ion activity coefficients of different Fe(II) species in carbonated seawater. The model fits available measurements of Fe(II)-oxidation in carbonated media at low (i.e., pure water) and high (i.e., I = 0.7 m, or seawater) ionic strength by specifying rate constants for individual Fe(II) species and calculating their weighted sum to determine the overall oxidation rate.

Figure DR3 shows the distribution of aqueous Fe(II) species in seawater with 100 µmol/kg total Fe^{2+}, 2.00 mmol/kg $SiO_2(aq)$, ionic strength = 0.7 m, $P_{CO2} = 10^{-2}$ bar (from Blättler et al., 2016), and T = 25°C. For all calculations, we assume that $SiO_2(aq)$ concentrations were near amorphous silica solubility, which is reflected by multiple generations of ubiquitous and early silicification of chemical sediments. The model shows that at pH values above 7, Fe(II)-carbonate species begin to dominate, which react at various rates with $O_2(aq)$.

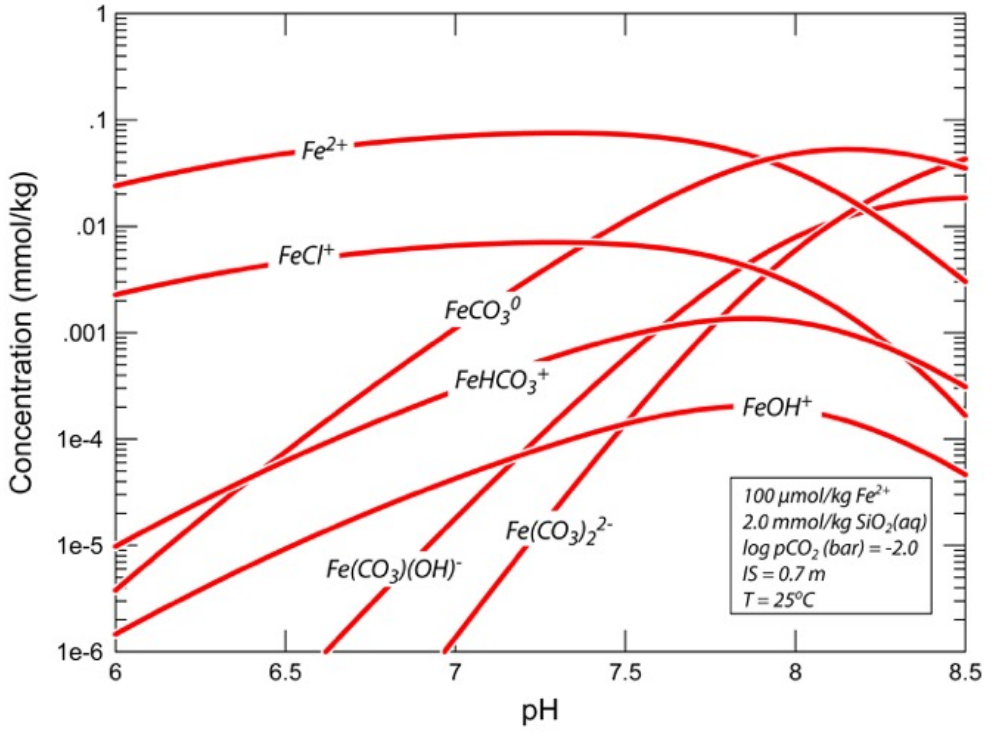

Fig. DR3. The distribution of aqueous Fe(II) species in Archean seawater as a function of pH. Model calculations show that at conservative estimates of P_{CO2} (i.e., Blättler et al., 2016), Fe(II)-carbonate species begin to dominate speciation and therefore Fe(II)-oxidation kinetics.

Figure 3 (main text) illustrates how the overall rates of Fe(II)-oxidation predicted by the model compare with measurements of Fe(II)-oxidation rates in carbonated modern seawater (9 mmol/kg HCO_3; Millero et al., 1987). In general. the model shows excellent agreement with laboratory measurements, especially at pH >6.

Quantitative comparison of greenalite precipitation and Fe^{2+}-oxidation rates

Figures DR4 to DR6 show comparisons of greenalite precipitation and Fe(II) oxidation rates as a function of pH and atmospheric O_2 content at three different total Fe concentrations: 10, 100 and 1000 µmol/kg Fe(II). Although the greenalite precipitation rates and Fe(II)-oxidation rates respond somewhat differently to Fe concentration, all three examples show that, under large ranges in pH and Fe concentration, low atmospheric $O_2(aq)$ is required in every case for greenalite precipitation to outpace Fe(II)-oxidation, and therefore generate and preserve sediments rich in greenalite. For example, at a total Fe(II) concentration of 100 µmol/kg, a P_{O2} of 10^{-6} x PAL would allow more rapid greenalite precipitation than Fe(II) oxidation only at high pH (above 7.75). In contrast, a P_{O2} of 10^{-7} x PAL would allow greenalite to form with little to no Fe-oxidation over a larger pH range (from pH 7.1 and higher) and therefore a larger and more commonly satisfied solution space. Repeating this comparison for other Fe concentrations results in large parameter spaces that are commonly defined by $P_{O2} < 10^{-6}$. The role of increasing dissolved CO_2 by one order of magnitude (i.e., to $P_{CO2} = 10^{-1}$ bar) has little effect on the outcome of the calculations (not shown). This is because Fe(II)-oxidation rates are calculated as a weighted average of all Fe(II) aqueous species, not their absolute abundances. Thus, at elevated P_{CO2}, further increases beyond this level translate to minor quantitative differences in Fe(II)-oxidation rates.

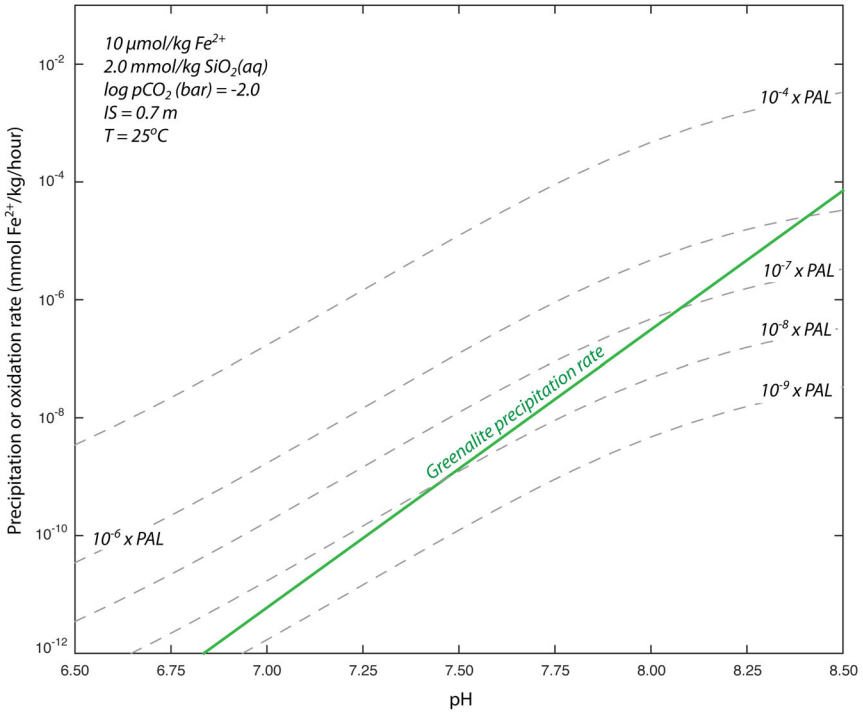

Fig. DR4. Comparison of greenalite versus Fe(II) oxidation rates as a function of pO_2 and pH (Fe^{2+} = 10 µmol/kg). The grey curves below the green line represent pO_2 values at which the rate of greenalite precipitation exceeds that of Fe(II) oxidation.

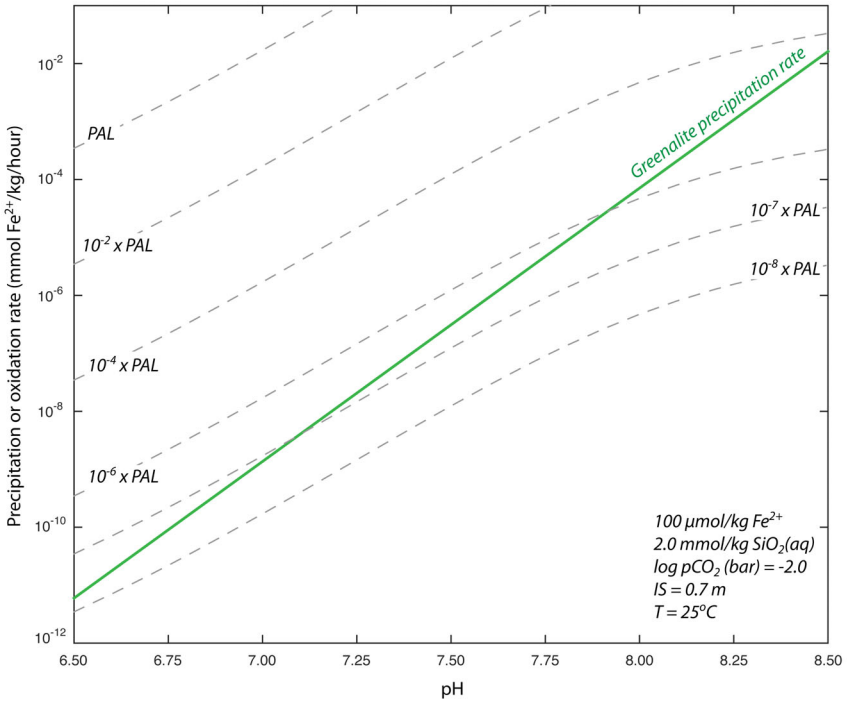

Fig. DR5. Comparison of greenalite versus Fe(II) oxidation rates as a function of pO_2 and pH (Fe^{2+} = 100 µmol/kg). The grey curves below the green line represent pO_2 values at which the rate of greenalite precipitation exceeds that of Fe(II) oxidation.

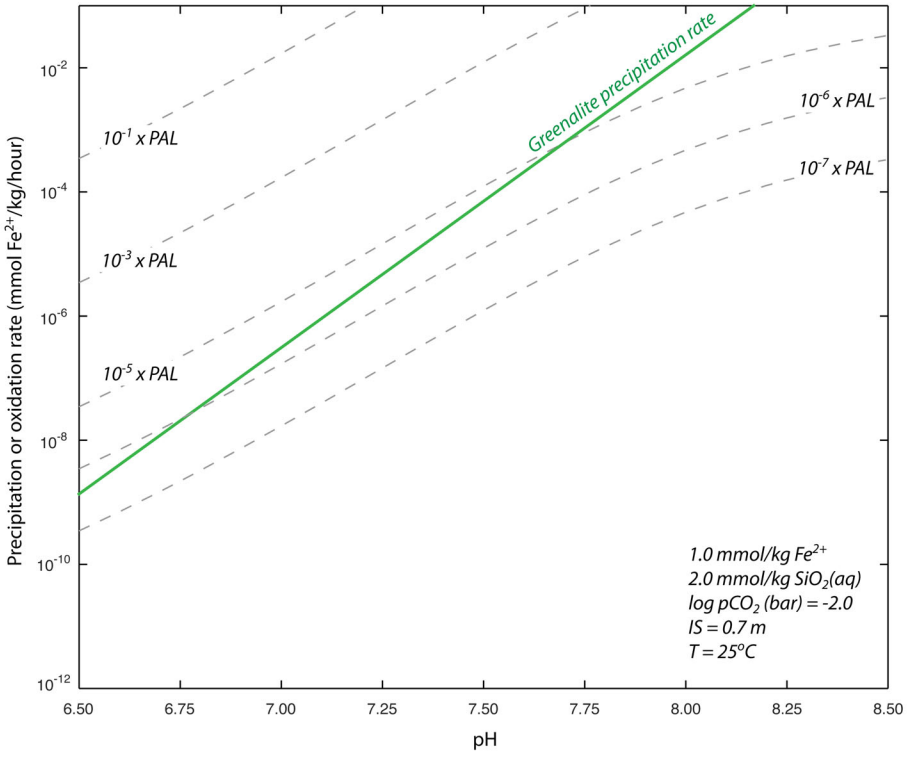

Fig. DR6. Comparison of greenalite versus Fe(II) oxidation rates as a function of pO_2 and pH (Fe^{2+} = 1000 µmol/kg). The grey curves below the green line represent pO_2 values at which the rate of greenalite precipitation exceeds that of Fe(II) oxidation.

Fe^{2+} photo-oxidation rates

The sedimentological, mineralogical, and geochemical evidence discussed here clearly indicate that shallow seawater on the shelf upon which the Griquatown Iron Formation was deposited was essentially devoid of dissolved $O_2(aq)$. However, one abiotic mechanism commonly hypothesized to have resulted in Fe(II) oxidation is UV photo-oxidation (Braterman et al., 1983; 1984; Braterman and Cairns-Smith, 1987). Braterman et al. (1984) hypothesized that at pH levels above 6.5, the photo-oxidation of Fe(II) is principally controlled by the photolysis of $FeOH^+$. However, their experiments were conducted in solutions containing NaCl as the only other dissolved components, neglecting the effects of dissolved CO_2. As discussed above, the presence of dissolved CO_2 and other dissolved components in Archean seawater would have promoted the formation of a number of aqueous Fe(II) complexes, which may have strongly influenced the photo activity of Fe in solution. In addition, these complexes would have decreased the concentration of $FeOH^+$ in solution and, therefore, the overall photo-oxidation rate of Fe(II). For example, using the Fe(II) speciation model described above, the concentration of $FeOH^+$ in seawater solutions decreases significantly in the presence of dissolved CO_2, an effect which would be anticipated to contribute to a decrease in photo-oxidation rates (Fig. DR7). In addition, the influence of other dissolved components on the efficiency (or quantum yield) on Fe(II) photochemistry has not been comprehensively evaluated. However, Konhauser et al. (2007), in experiments designed to examine the competition between UV photo-oxidation of Fe(II) and the anoxic precipitation of Fe(II)-minerals from Archean seawater rich in CO_2, observed that Fe(II) minerals precipitated at rates far higher than UV photo-oxidation. They further observed that Fe(II) photo-oxidation rates were significantly lower than predicted by Braterman et al. (1984)'s study. These results indicate that the combined influences of multi-component seawater solutions on complexation (therefore yielding lower $FeOH^+$ concentrations) and possibly a reduced quantum yield, translate to negligible UV photo-oxidation rates of Fe(II) from Archean seawater residing in the photic zone.

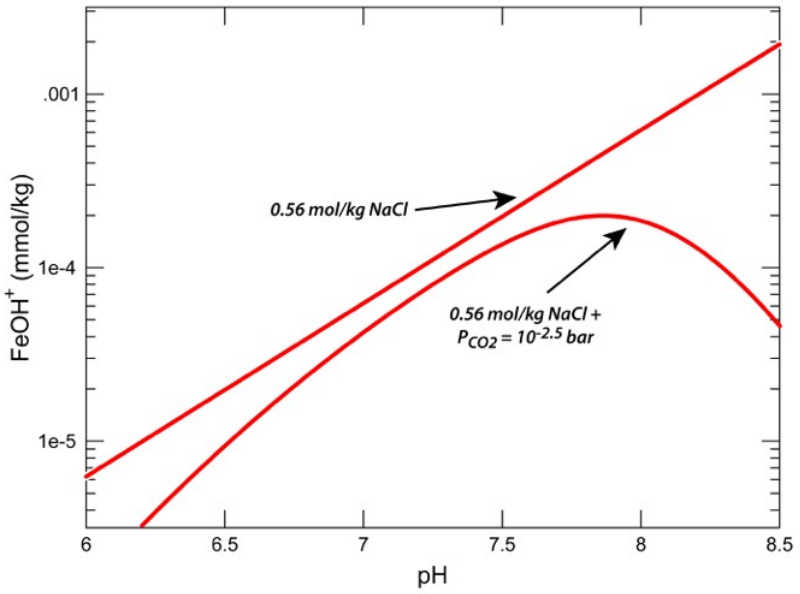

Fig. DR7. The effect of dissolved CO_2 on the total concentration of $FeOH^+$, the principal photoactive species of Fe(II), in Archean seawater. Model calculations show that the presence of dissolved CO_2 alone leads to a significant reduction in seawater $FeOH^+$ concentrations and therefore Fe(II) photo-oxidation rates.

REFERENCES CITED

Blättler, C.L., Kump, L.R., Fischer, W.W., Paris, G., Kasbohm, J.J., and Higgins, J.A., 2017, Constraints on ocean carbonate chemistry and pCO_2 in the Archaean and Palaeoproterozoic: Nature Geoscience, v. 10, p. 41-47. doi:10.1038/NGEO2844.

Braterman, P.S., Cairns-Smith, A.G., and Sloper, R.W., 1983, Photo-oxidation of hydrated Fe^{2+}-significance for banded iron formations: Nature, v. 303, p. 163-164.

Braterman, P.S., Cairns-Smith, A.G., and Sloper, R.W., 1984, Photo-oxidation of iron(II) in water between pH 7.5 and 4.0: Journal of the Chemical Society, Dalton Transactions, 1441-1445.

Braterman, P.S., and Cairns-Smith, A.G., 1987, Photoprecipitation and the banded iron-formations - Some quantitative aspects: Origins of Life and Evolution of the Biosphere, v. 17, p. 221-228.

King, D.W., 1998, Role of carbonate speciation on the oxidation rate of Fe(II) in aquatic systems: Environmental Science and Technology, v. 32, p. 2997-3003.

Konhauser, K.O., et al., 2007, Decoupling photochemical Fe (II) oxidation from shallow-water BIF deposition: Earth and Planetary Science Letters, v. 258, p. 87-100. doi:10.1016/j.epsl.2007.03.026.

Lasaga, A.C., 1998, *Kinetic Theory in the Earth Sciences*, Holland, H.D., eds, (Princeton University Press, Princeton, NJ) 811 p.

Millero, F.J., Sotolongo S., and Izaguirre M., 1987, The oxidation kinetics of Fe(II) in seawater: Geochimica et Cosmochimica Acta, v. 51, p. 793-801.

Millero, F.J., and Izaguirre, M., 1989, Effect of ionic strength and ionic interactions on the oxidation of Fe(II): Journal of Solution Chemistry, v. 18, p. 585-598.

Tosca, N.J., Guggenheim, S., and Pufahl, P.K., 2016, An authigenic origin for Precambrian greenalite: Implications for iron formation and the chemistry of ancient seawater: Geological Society of America Bulletin, v. 128, p. 511-530. doi:10.1130/B31339.1.

Wehrli, B., 1990, Redox reactions of metal ions at mineral surfaces. In *Aquatic Chemical Kinetics* (pp. 311-336), Wiley-Interscience.